

# Phenomenological Profiles of the Inclusive Hadron Spectra in the Decay $B \rightarrow X_s \ell^+ \ell^-$

A. Ali\* and G. Hiller†

Deutsches Elektronen-Synchrotron DESY, Hamburg

## Abstract

Hadron spectra and hadronic moments in the decay  $B \rightarrow X_s \ell^+ \ell^-$  are calculated taking into account both the short-distance and long-distance contributions in the decay amplitude using a Fermi motion (FM) model to incorporate the  $B$ -meson wave-function effects. The measured branching ratios for the inclusive decays  $B \rightarrow X_s + (J/\psi, \psi', \dots) \rightarrow X_s \ell^+ \ell^-$  are used to fix the normalization of the long-distance contribution. The momentum distribution of the  $J/\psi$  measured by the CLEO collaboration is fitted in the FM model which is then used to calculate the hadronic spectra from the resonant contribution also away from the  $J/\psi$ -resonance. We also study the effect of various descriptions of the resonant and non-resonant  $c\bar{c}$  contributions in  $B \rightarrow X_s \ell^+ \ell^-$  existing in the literature on the hadron energy and invariant mass spectra, and in the Forward-Backward asymmetry. Selective cuts on the hadron and dilepton invariant masses can be used to reduce the  $B\bar{B}$  background and resonant contribution and, as an example, we work out the hadron spectra with the experimental cuts used by the CLEO collaboration in searching for the decay  $B \rightarrow X_s \ell^+ \ell^-$ . We show that data from the forthcoming B facilities could be used effectively to measure the short-distance contribution in  $B \rightarrow X_s \ell^+ \ell^-$ , enabling precise determination of the FM model and heavy quark effective theory parameters  $\lambda_1$  and  $\bar{\Lambda}$ .

(Submitted to Physical Review D)

---

\*E-mail address: ali@x4u2.desy.de

†E-mail address: ghiller@x4u2.desy.de

# 1 Introduction

In two earlier papers [1,2], we have worked out the short-distance (SD) contribution to the hadron energy and hadronic invariant mass spectra and the first two spectral moments in the inclusive decay  $B \rightarrow X_s \ell^+ \ell^-$ . The calculations reported in these papers were based on the leading order perturbative QCD corrections in  $\alpha_s$  and leading power corrections in  $1/m_b^2$  using the heavy quark expansion technique (HQET) [3,4]. In particular, we worked out the dependence of the moments  $\langle S_H^n \rangle$  and  $\langle E_H^n \rangle$ , for  $n = 1, 2$ , valid up to  $\mathcal{O}(\alpha_s/m_B^2, 1/m_B^3)$ . It was argued that their measurements in forthcoming experiments could be combined with the improved measurements of the same in the semileptonic decays  $B \rightarrow X \ell \nu_\ell$  to determine the HQET parameters  $\lambda_1$  and  $\bar{\Lambda}$  precisely. Since these parameters are endemic to most applications of HQET, their precise determination would reduce the present theoretical uncertainties improving the standard model calculations. In particular, the determinations of the CKM matrix elements  $V_{ub}$  and  $V_{cb}$  would be considerably improved. The correlations resulting from (assumed) values of  $\langle S_H \rangle$  and  $\langle S_H^2 \rangle$  were shown and compared with the constraints emerging from the analysis of the decay  $B \rightarrow X \ell \nu_\ell$  reported in [5]. The hadron spectra and spectral moments were also calculated in a phenomenological Fermi motion model (FM) [6]. In particular, the remarkable similarity of the hadronic moments in the HQET and FM model approaches was quantified. Finally, the effects of the experimental cuts on the spectra used in the searches for the decay  $B \rightarrow X_s \ell^+ \ell^-$  by the CLEO collaboration [7] were studied. However, the effects of the long-distance contributions were not included in the hadron spectra or the spectral moments.

The aim of this paper is to calculate the profile of hadron energy and invariant mass spectra by incorporating the effects of the long-distance (LD) contributions in the decay  $B \rightarrow X_s \ell^+ \ell^-$ . As opposed to the SD-contribution discussed in [1,2], the LD-contributions are estimated phenomenologically. To that end, the branching ratios for  $B \rightarrow (J/\psi, \psi', \dots) + X_s \rightarrow X_s \ell^+ \ell^-$  are described in the factorization approach [8–9], with the data fixing the normalization and phase of the LD-contribution in  $B \rightarrow X_s \ell^+ \ell^-$  at the  $J/\psi, \psi', \dots$  resonances [10]. Assuming a Breit-Wigner form, one can extrapolate the dilepton mass spectra away from the  $J/\psi, \psi', \dots$  resonances. Using this and the SD-contribution, various distributions in  $B \rightarrow X_s \ell^+ \ell^-$  have been worked out in the literature [10–16]. We use the FM model to incorporate the wave-function effects. In the process of doing this, we also show that the FM model [6] provides an adequate description of the  $J/\psi$ -momentum distribution in the decay  $B \rightarrow J/\psi + X_s \rightarrow X_s \ell^+ \ell^-$  measured by the CLEO collaboration [17]. This confirms a similar and earlier study on this point [18]. However, we have redone a fit of the CLEO-data on the  $J/\psi$ -momentum spectrum and prefer somewhat different FM model parameters than the ones presented in [18], motivated by the analysis of the photon energy spectrum in the decay  $B \rightarrow X_s + \gamma$  [19] and theoretical consideration on the  $b$ -quark mass [20].

The prescription of adding the SD and LD-contributions in the decay  $B \rightarrow X_s \ell^+ \ell^-$  is not unique, which introduces a theoretical dispersion in the resulting spectra. Related to this is the inherent uncertainty concerning the extrapolation of the resonant part far away from the resonances [11,13,14]. We study these uncertainties by working out a number of Ansätze used in the literature. The dispersion on the spectra emerging from various approaches can then be taken as a measure of theoretical systematic errors from these sources. We analyze the dilepton invariant mass distribution, the Forward Backward (FB) asymmetry, hadron energy and hadronic invariant mass spectra and the hadron spectral moments in this context. The LD/SD-related uncertainties are found to be small for the hadron spectra and spectral moments. Some of these issues were also discussed in the context of exclusive decays  $B \rightarrow (K, K^*) \ell^+ \ell^-$  in the second reference cited in [16].

Finally, we study the effect of experimental cuts on the branching ratios, hadron spectra and spectral moments in  $B \rightarrow X_s \ell^+ \ell^-$ . For that purpose we take the cuts used by the CLEO collaboration [7], which involve dilepton and hadronic invariant masses. We present a comparative analysis of these cuts on the inclusive hadron energy and invariant hadronic mass distributions with and without the  $c\bar{c}$ -resonant contributions. This shows that the cuts employed in [7] are effective in removing the resonant part and given data one could study the more interesting SD-contribution in  $B \rightarrow X_s \ell^+ \ell^-$ .

This paper is organized as follows: In section 2, we define the kinematics of the process  $B \rightarrow X_s \ell^+ \ell^-$  and introduce the quantities of dynamical interest in the framework of an effective Hamiltonian. Section 3 describes the wave-function effects in the FM model [6] in the hadron energy and hadronic invariant mass spectra. The resulting inclusive hadron spectra in  $B \rightarrow X_s \ell^+ \ell^-$ , including the long-distance effects in terms of the  $J/\psi, \psi', \dots$  resonances, are presented. Comparison with the  $J/\psi$ -momentum spectrum measured by the CLEO collaboration is shown, constraining the FM model parameters. Theoretical uncertainties in the effective coefficients  $\text{Re } C_9^{\text{eff}}$  and  $|C_9^{\text{eff}}|$  from the various prescriptions are displayed here and the resulting spectra in hadron energy, dilepton invariant mass and the FB-asymmetry are presented. Hadronic spectral moments are calculated in the FM model taking into account the LD contributions. Comparison with the corresponding quantities derived from the SD-contribution alone using the HQET and FM models in [1,2] is also presented. In section 4, the effects of the experimental cuts used in the CLEO analysis of  $B \rightarrow X_s \ell^+ \ell^-$  are studied and the resulting spectra are presented in terms of several figures. Estimates of the branching ratios  $\mathcal{B}(B \rightarrow X_s \ell^+ \ell^-)$  for  $\ell = e, \mu$  are also presented here, together with estimates of the survival probability for the CLEO cuts, using the FM model. Section 5 contains a summary of our work and some concluding remarks.

## 2 The Decay $B \rightarrow X_s \ell^+ \ell^-$ in the Effective Hamiltonian Approach

## 2.1 Kinematics

The kinematics for the decay in question at the partonic and hadronic level are defined in [1,2]. Hence, we will be short here. The parton level kinematics is given by

$$b(p_b) \rightarrow s(p_s)(+g(p_g)) + \ell^+(p_+) + \ell^-(p_-) , \quad (1)$$

where  $g$  denotes a gluon from the  $O(\alpha_s)$  correction. The corresponding kinematics at the hadron level is defined as:

$$B(p_B) \rightarrow X_s(p_H) + \ell^+(p_+) + \ell^-(p_-) . \quad (2)$$

We define the momentum transfer to the lepton pair and the invariant mass of the dilepton system, respectively, as

$$q \equiv p_+ + p_- , \quad (3)$$

$$s \equiv q^2 . \quad (4)$$

Further, we define a 4-vector  $v$ , which denotes the velocity of both the  $b$ -quark and the  $B$ -meson,  $p_b = m_b v$  and  $p_B = m_B v$ . The hadronic invariant mass is denoted by  $S_H \equiv p_H^2$  and  $E_H$  denotes the hadron energy in the final state. The corresponding quantities at parton level are the invariant mass  $s_0$  and the scaled parton energy  $x_0 \equiv \frac{E_0}{m_b}$ . In parton model without gluon bremsstrahlung, this simplifies to  $s_0 = m_s^2$  and  $x_0$  becomes directly related to the dilepton invariant mass  $x_0 = 1/2(1 - \hat{s} + \hat{m}_s^2)$ . Here and in what follows, the dimensionless variables with a hat are related to the dimensionful variables by the scale  $m_b$ , the  $b$ -quark mass, e.g.,  $\hat{s} = \frac{s}{m_b^2}$ ,  $\hat{m}_s = \frac{m_s}{m_b}$  etc. From momentum conservation the following equalities hold in the  $b$ -quark, equivalently  $B$ -meson, rest frame ( $v = (1, 0, 0, 0)$ ):

$$\begin{aligned} x_0 &= 1 - v \cdot \hat{q} , \\ \hat{s}_0 &= 1 - 2v \cdot \hat{q} + \hat{s} , \end{aligned} \quad (5)$$

$$\begin{aligned} E_H &= m_B - v \cdot q , \\ S_H &= m_B^2 - 2m_B v \cdot q + s . \end{aligned} \quad (6)$$

The relation between the kinematic variables of the parton model and the hadronic states can be seen in [1,2].

## 2.2 Matrix element for the decay $B \rightarrow X_s \ell^+ \ell^-$

The effective Hamiltonian obtained by integrating out the top quark and the  $W^\pm$  bosons is given as

$$\begin{aligned} \mathcal{H}_{eff}(b \rightarrow s + X, X = \gamma, \ell^+ \ell^-) = & -\frac{4G_F}{\sqrt{2}} V_{ts}^* V_{tb} \left[ \sum_{i=1}^6 C_i(\mu) O_i + C_7(\mu) \frac{e}{16\pi^2} \bar{s}_\alpha \sigma_{\mu\nu} (m_b R + m_s L) b_\alpha F^{\mu\nu} \right. \\ & \left. + C_8(\mu) O_8 + C_9(\mu) \frac{e^2}{16\pi^2} \bar{s}_\alpha \gamma^\mu L b_\alpha \bar{\ell} \gamma_\mu \ell + C_{10} \frac{e^2}{16\pi^2} \bar{s}_\alpha \gamma^\mu L b_\alpha \bar{\ell} \gamma_\mu \gamma_5 \ell \right] , \quad (7) \end{aligned}$$

where  $L$  and  $R$  denote chiral projections,  $L(R) = 1/2(1 \mp \gamma_5)$ ,  $V_{ij}$  are the CKM matrix elements and the CKM unitarity has been used in factoring out the product  $V_{ts}^* V_{tb}$ . The operator basis is taken from [10], where also the Four-Fermi operators  $O_1, \dots, O_6$  and the chromomagnetic operator  $O_8$  can be seen. Note that  $O_8$  does not contribute to the decay  $B \rightarrow X_s \ell^+ \ell^-$  in the approximation which we use here. The  $C_i(\mu)$  are the Wilson coefficients, which depend, in general, on the renormalization scale  $\mu$ , except for  $C_{10}$ .

The matrix element for the decay  $B \rightarrow X_s \ell^+ \ell^-$  can be factorized into a leptonic and a hadronic part as

$$\mathcal{M}(B \rightarrow X_s \ell^+ \ell^-) = \frac{G_F \alpha}{\sqrt{2} \pi} V_{ts}^* V_{tb} \left( \Gamma_{\mu}^L L^{L\mu} + \Gamma_{\mu}^R L^{R\mu} \right), \quad (8)$$

with

$$L^{L/R}_{\mu} \equiv \bar{\ell} \gamma_{\mu} L(R) \ell, \quad (9)$$

$$\Gamma_{\mu}^{L/R} \equiv \bar{s} \left[ R \gamma_{\mu} \left( C_9^{\text{eff}}(\hat{s}) \mp C_{10} + 2C_7^{\text{eff}} \frac{\hat{q}}{\hat{s}} \right) + 2\hat{m}_s C_7^{\text{eff}} \gamma_{\mu} \frac{\hat{q}}{\hat{s}} L \right] b. \quad (10)$$

The effective Wilson coefficient  $C_9^{\text{eff}}(\hat{s})$  receives contributions from various pieces. Since the resonant  $c\bar{c}$  states also contribute to  $C_9^{\text{eff}}(\hat{s})$ , the contribution given below is just the perturbative part:

$$C_9^{\text{eff}}(\hat{s})|_{\text{pert}} = C_9 \eta(\hat{s}) + Y(\hat{s}). \quad (11)$$

Here  $\eta(\hat{s})$  and  $Y(\hat{s})$  represent the  $\mathcal{O}(\alpha_s)$  correction [21] and the one loop matrix element of the Four-Fermi operators [22,23], respectively. While  $C_9$  is a renormalization scheme-dependent quantity, this dependence cancels out with the corresponding one in the function  $Y(\hat{s})$  (the value of  $\xi$ , see below). To be self-contained, we list the two functions in  $C_9^{\text{eff}}(\hat{s})$ :

$$\begin{aligned} Y(\hat{s}) &= g(\hat{m}_c, \hat{s}) (3C_1 + C_2 + 3C_3 + C_4 + 3C_5 + C_6) \\ &\quad - \frac{1}{2} g(1, \hat{s}) (4C_3 + 4C_4 + 3C_5 + C_6) - \frac{1}{2} g(0, \hat{s}) (C_3 + 3C_4) \\ &\quad + \frac{2}{9} (3C_3 + C_4 + 3C_5 + C_6) - \xi \frac{4}{9} (3C_1 + C_2 - C_3 - 3C_4), \end{aligned} \quad (12)$$

$$\eta(\hat{s}) = 1 + \frac{\alpha_s(\mu)}{\pi} \omega(\hat{s}), \quad (13)$$

$$\xi = \begin{cases} 0 & \text{(NDR)}, \\ -1 & \text{(HV)}, \end{cases} \quad (14)$$

$$\begin{aligned} g(z, \hat{s}) &= -\frac{8}{9} \ln\left(\frac{m_b}{\mu}\right) - \frac{8}{9} \ln z + \frac{8}{27} + \frac{4}{9} y - \frac{2}{9} (2+y) \sqrt{|1-y|} \\ &\quad \times \left[ \Theta(1-y) \left( \ln \frac{1+\sqrt{1-y}}{1-\sqrt{1-y}} - i\pi \right) + \Theta(y-1) 2 \arctan \frac{1}{\sqrt{y-1}} \right], \end{aligned} \quad (15)$$

$$g(0, \hat{s}) = \frac{8}{27} - \frac{8}{9} \ln\left(\frac{m_b}{\mu}\right) - \frac{4}{9} \ln \hat{s} + \frac{4}{9} i\pi, \quad (16)$$

where  $y = 4z^2/\hat{s}$ , and

$$\begin{aligned} \omega(\hat{s}) &= -\frac{2}{9}\pi^2 - \frac{4}{3}\text{Li}_2(\hat{s}) - \frac{2}{3}\ln \hat{s} \ln(1 - \hat{s}) - \frac{5 + 4\hat{s}}{3(1 + 2\hat{s})} \ln(1 - \hat{s}) \\ &- \frac{2\hat{s}(1 + \hat{s})(1 - 2\hat{s})}{3(1 - \hat{s})^2(1 + 2\hat{s})} \ln \hat{s} + \frac{5 + 9\hat{s} - 6\hat{s}^2}{6(1 - \hat{s})(1 + 2\hat{s})} . \end{aligned} \quad (17)$$

Above, (NDR) and (HV) correspond to the naive dimensional regularization and the 't Hooft-Veltman schemes, respectively. Note that the function  $g(\hat{m}_c, \hat{s})(3C_1 + C_2 + \dots)$  given above is the perturbative contribution to the effective coefficient  $C_9^{\text{eff}}(\hat{s})$  from the  $c\bar{c}$  loop, to which we have referred in the introduction and to whose discussion we shall return in section 3. The other Wilson coefficients in leading logarithmic approximation can be seen in [22].

Parameter	Value
$m_W$	80.26 (GeV)
$m_Z$	91.19 (GeV)
$\sin^2 \theta_W$	0.2325
$m_s$	0.2 (GeV)
$m_c$	1.4 (GeV)
$m_b$	4.8 (GeV)
$m_t$	$175 \pm 5$ (GeV)
$\mu$	$m_b^{+m_b} - m_b/2$
$\Lambda_{QCD}^{(5)}$	$0.214_{-0.054}^{+0.066}$ (GeV)
$\alpha^{-1}$	129
$\alpha_s(m_Z)$	$0.117 \pm 0.005$
$\mathcal{B}_{sl}$	$(10.4 \pm 0.4)$ %
$\lambda_1$	$-0.20$ (GeV <sup>2</sup> )
$\lambda_2$	$+0.12$ (GeV <sup>2</sup> )

Table 1: *Default values of the input parameters and errors used in the numerical calculations.*

$C_1$	$C_2$	$C_3$	$C_4$	$C_5$	$C_6$	$C_7^{\text{eff}}$	$C_9$	$C_{10}$	$C^{(0)}$
-0.240	+1.103	+0.011	-0.025	+0.007	-0.030	-0.311	+4.153	-4.546	+0.381

Table 2: *Values of the Wilson coefficients used in the numerical calculations corresponding to the central values of the parameters given in Table 1. For  $C_9$  we use the NDR scheme.*

### 3 Hadron Spectra in $B \rightarrow X_s \ell^+ \ell^-$ in the Fermi Motion Model Including Long-Distance Contribution

In this section, we study non-perturbative effects associated with the bound state nature of the  $B$  hadron and of the  $c\bar{c}$  resonances  $B \rightarrow X_s + (J/\psi, \psi', \dots) \rightarrow X_s \ell^+ \ell^-$  (the LD contribution) on the

hadronic invariant mass and hadron energy distributions in the decay  $B \rightarrow X_s \ell^+ \ell^-$ . Wave-function effects are studied in the FM model [6] and for the resonant part we use data. The FM model parameters are then constrained from the measured  $J/\psi$ -momentum spectrum [17]. Sensitivity of the inclusive spectra in  $B \rightarrow X_s \ell^+ \ell^-$  on the assumed resonant and the perturbative  $c\bar{c}$ -contribution is presented. The hadronic spectral moments  $\langle X_H^n \rangle$ , with  $X = S, E$  and  $n = 1, 2$ , are calculated numerically in the FM model including the LD-effects. For the sake of comparison, the corresponding quantities calculated for the SD-contribution using HQET and the FM model from [2] are also given.

### 3.1 Hadron spectra in $B \rightarrow X_s \ell^+ \ell^-$ in the Fermi motion model

The FM model often invoked in phenomenological studies of  $B$  decays [6] has two parameters  $p_F$ , the Fermi momentum of the  $b$ -quark, and the spectator quark mass  $m_q$ . Energy-momentum conservation requires the  $b$ -quark mass to be a momentum-dependent parameter determined by the constraint:

$$m_b^2(p) = m_B^2 + m_q^2 - 2m_B \sqrt{p^2 + m_q^2} \quad ; \quad p = |\vec{p}|. \quad (18)$$

The  $b$ -quark momentum  $p$  is assumed to have a Gaussian distribution, denoted by  $\phi(p)$ , which is determined by  $p_F$

$$\phi(p) = \frac{4}{\sqrt{\pi} p_F^3} \exp\left(\frac{-p^2}{p_F^2}\right), \quad (19)$$

with the normalization  $\int_0^\infty dp p^2 \phi(p) = 1$ . In this model, the HQET parameters  $\bar{\Lambda}$  and  $\lambda_1$ , representing, respectively, the binding energy and the kinetic energy of the  $b$ -quark inside a  $B$  meson, are calculable in terms of  $p_F$  and  $m_q$  with

$$\begin{aligned} \bar{\Lambda} &= \int_0^\infty dp p^2 \phi(p) \sqrt{m_q^2 + p^2}, \\ \lambda_1 &= - \int_0^\infty dp p^4 \phi(p) = -\frac{3}{2} p_F^2. \end{aligned} \quad (20)$$

In addition, for  $m_q = 0$ , one can show that  $\bar{\Lambda} = 2p_F/\sqrt{\pi}$ . There is, however, no analog of  $\lambda_2$  in the FM model. For subsequent use in working out the normalization (decay widths) in the FM model, we also define an *effective*  $b$ -quark mass by

$$m_b^{\text{eff}} \equiv \left( \int_0^\infty dp p^2 m_b(p)^5 \phi(p) \right)^{1/5}. \quad (21)$$

With the quantities  $m_b^{\text{eff}}$ ,  $\lambda_1$  and  $\bar{\Lambda}$  defined above, the relation

$$m_B = m_b^{\text{eff}} + \bar{\Lambda} - \lambda_1 / (2m_b^{\text{eff}}), \quad (22)$$

is found to be satisfied in the FM model to a high accuracy (within 0.7%), which is shown in Table 3 for some representative values of the HQET parameters and their FM model equivalents. We shall use the HQET parameters  $\bar{\Lambda}$  and  $\lambda_1$  to characterize also the FM model parameters, with the relations given in eqs. (20) and (21) and in Table 3.

$p_F, m_q$ (MeV, MeV)	$m_b^{\text{eff}}$ (GeV)	$\lambda_1$ (GeV <sup>2</sup> )	$\bar{\Lambda}$ (GeV)
(450, 0)	4.76	-0.304	0.507
(252, 300)	4.85	-0.095	0.422
(310, 0)	4.92	-0.144	0.350
(450, 150)	4.73	-0.304	0.534
(500, 150)	4.68	-0.375	0.588
(570, 150)	4.60	-0.487	0.664

Table 3: Values of non perturbative parameters  $m_b^{\text{eff}}$ ,  $\lambda_1$  and  $\bar{\Lambda}$  defined in the FM model for different sets of the FM model parameters ( $p_F, m_q$ ).

### 3.2 Long-distance resonant contribution in $B \rightarrow X_s \ell^+ \ell^-$

If not stated otherwise, we shall follow the procedure adopted in [10], in which the long-distance (LD) resonance effects in the decay  $B \rightarrow X_s \ell^+ \ell^-$  (specified below) are added with the perturbative  $c\bar{c}$  contribution expressed through the function  $g(\hat{m}_c, \hat{s})$  in section 2 (see, eq. (15)). Thus,

$$C_9^{\text{eff}}(\hat{s}) = C_9 \eta(\hat{s}) + Y(\hat{s}) + Y_{res}(\hat{s}) . \quad (23)$$

The function  $Y_{res}(\hat{s})$  accounts for the charmonium resonance contribution via  $B \rightarrow X_s(J/\Psi, \Psi', \dots) \rightarrow X_s \ell^+ \ell^-$  for which we take the representation [11],

$$Y_{res}(\hat{s}) = \frac{3}{\alpha^2} \kappa C^{(0)} \sum_{V_i=\psi(1s), \dots, \psi(6s)} \frac{\pi \Gamma(V_i \rightarrow \ell^+ \ell^-) M_{V_i}}{M_{V_i}^2 - \hat{s} m_b^2 - i M_{V_i} \Gamma_{V_i}}, \quad (24)$$

where  $C^{(0)} \equiv 3C_1 + C_2 + 3C_3 + C_4 + 3C_5 + C_6$ . We adopt  $\kappa = 2.3$  for the numerical calculations [24]. This is a fair representation of present data in the factorization approach [25]; also the phase of  $\kappa$ , which is fixed in eq. (24), is now supported by data which finds it close to its perturbative value [9]. Note that in this approach, the effective coefficient  $C_9^{\text{eff}}(\hat{s})$  has a  $\hat{s}$ -dependence, which is not entirely due to the propagators in the function  $Y_{res}(\hat{s})$  as also the perturbative  $c\bar{c}$  contribution  $g(\hat{m}_c, \hat{s})$  is a function of  $\hat{s}$ . In the resonant region, the perturbative part is not noticeable due to the fact that the resonant part in  $C_9^{\text{eff}}(\hat{s})$  completely dominates. However, when the  $c\bar{c}$  pair is sufficiently off-shell, the  $\hat{s}$ -dependence of the function  $C_9^{\text{eff}}(\hat{s})$  is not (and should not be) entirely determined by the  $c\bar{c}$  resonant contribution. This is the motivation of the representation in eq. (23). We shall later evaluate the uncertainties in various distributions arising from varying definitions of the perturbative contribution  $g(\hat{m}_c, \hat{s})$  as well as the precise form of the resonating contribution.

### 3.3 Constraints on the FM model parameters from existing data

The FM model parameters  $p_F$  and  $m_q$  (equivalently  $\lambda_1$  and  $\bar{\Lambda}$ ) for the SD-contribution can, in principle, be determined from an analysis of the energy spectra in the decays  $B \rightarrow X_u \ell \nu_\ell$  and  $B \rightarrow X_s + \gamma$ , as all



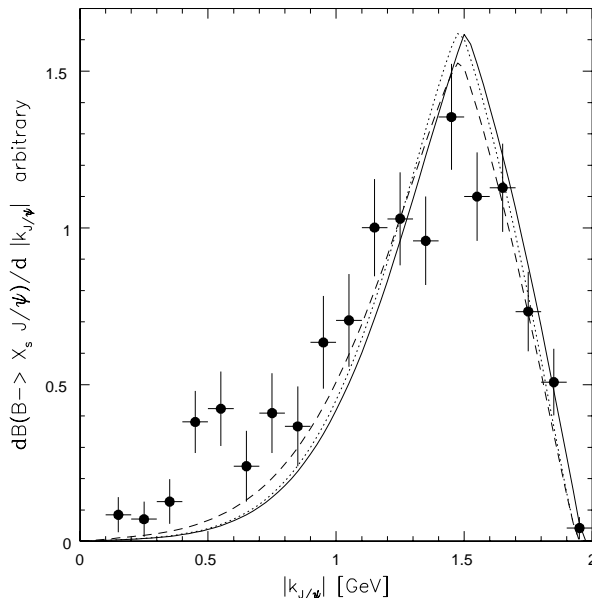


Figure 1: *Momentum distribution of  $J/\psi$  in the decay  $B \rightarrow X_s J/\psi$  in the FM model. The solid, dotted, dashed curve corresponds to the parameters  $(\lambda_1, \bar{\Lambda}) = (-0.3, 0.5), (-0.3, 0.53), (-0.38, 0.59)$  in  $(\text{GeV}^2, \text{GeV})$ , respectively. The data points are from the CLEO measurements [17].*

of them involve the decay of a  $b$  quark into (an almost) massless ( $u$  or  $s$ ) quark. However, the quality of the present data on  $B \rightarrow X_s + \gamma$  does not allow to draw very quantitative conclusions, and hence we vary the parameters in a reasonable range giving a satisfactory description of the photon energy spectrum and show the resulting uncertainties on the hadron spectra in  $B \rightarrow X_s \ell^+ \ell^-$ . For estimating the spectra from the LD contribution involving the transition  $b \rightarrow c$ , the parameters of the FM model can be constrained from the lepton energy spectrum in the decay  $B \rightarrow X_c \ell \nu_\ell$  and from the shape of the  $J/\psi$ - and  $\psi'$ - momentum distributions in the decays  $B \rightarrow X_s(J/\psi, \psi')$ . We review below the presently available analyses of the photon- and lepton-energy spectra in  $B$  decays in the FM model and also present an analysis of the  $J/\psi$ -momentum spectrum in  $B \rightarrow X_s J/\psi$ .

- Analysis of the photon energy spectrum in  $B \rightarrow X_s + \gamma$

The photon energy- and invariant hadronic mass distributions in  $B \rightarrow X_s \gamma$  were calculated in the FM model using the leading order (in  $\alpha_s$ ) corrections in ref. [26]. These spectra were used in the analysis of the CLEO data on  $B \rightarrow X_s + \gamma$  [27], in which the values  $p_F = 270 \pm 40$  MeV suggested by the analysis of the CLEO data on  $B \rightarrow X \ell \nu_\ell$  were used, together with the effective  $b$ -quark mass  $m_b^{\text{eff}} = 4.87 \pm 0.10$  GeV, which gave reasonable fits of the data. We translate these parameters in terms of  $\lambda_1$  and  $\bar{\Lambda}$  using the relations given in eqs. (20) and (22), yielding

$$\lambda_1 = -0.11_{-0.035}^{+0.030} \text{ GeV}^2, \quad \bar{\Lambda} = 0.40 \pm 0.1 \text{ GeV} . \quad (25)$$

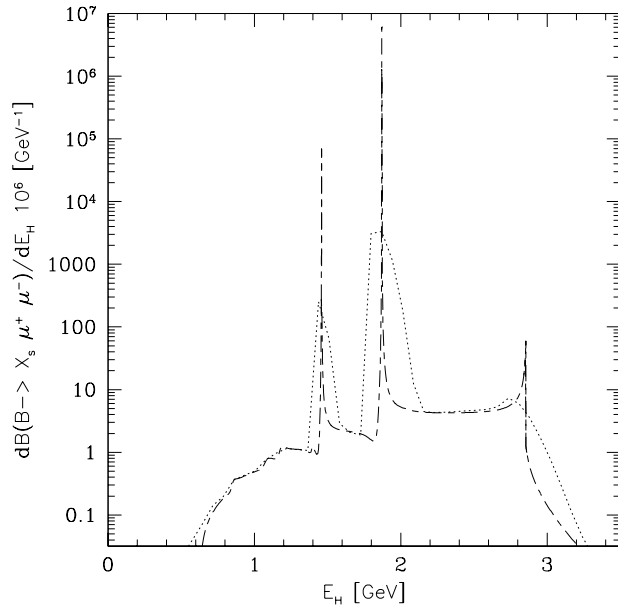


Figure 2: *Hadron energy spectrum in  $B \rightarrow X_s \ell^+ \ell^-$  including the resonant ( $J/\psi, \psi', \dots$ ) and perturbative contributions in the Fermi motion model (dotted curve) for  $(\lambda_1, \bar{\Lambda}) = (-0.1 \text{ GeV}^2, 0.4 \text{ GeV})$ , and in the parton model (long-short dashed curve) for  $m_b = 4.85 \text{ GeV}$ .*

The same data was fitted in ref. [19] in the FM model, yielding  $(p_F, m_q) = (0.45 \text{ GeV}, 0 \text{ GeV})$  as the best-fit solution, with  $(p_F, m_q) = (0.310 \text{ GeV}, 0.3 \text{ GeV})$  differing from the best-fit solution by one unit in  $\chi^2$ . The best-fit values translate into

$$\lambda_1 = -0.3 \text{ GeV}^2, \quad \bar{\Lambda} = 0.5 \text{ GeV}. \quad (26)$$

Within the indicated errors, the values given in eqs. (25) and (26) are compatible.

- Analysis of the lepton energy spectrum in  $B \rightarrow X \ell \nu_\ell$

A fit of the lepton energy spectrum in the semileptonic decay  $B \rightarrow X \ell \nu_\ell$  in the context of HQET has been performed in ref. [5]. Using the CLEO data [28], the authors of ref. [5] find:

$$\lambda_1 = -0.19 \pm 0.10 \text{ GeV}^2, \quad \bar{\Lambda} = 0.39 \pm 0.11 \text{ GeV}. \quad (27)$$

Since the FM model and HQET yield very similar lepton energy spectra (apart from the end-point), one can take the analysis of [5] also holding approximately for the FM model.

- Analysis of the  $J/\psi$ -momentum spectrum in  $B \rightarrow X_s J/\psi$

An analysis of the  $J/\psi$ -momentum spectrum in  $B \rightarrow X_s(J/\psi, \psi')$  measured by the CLEO collaboration [17] has been reported in ref. [18] using the FM model. The authors of ref. [18] addressed both the

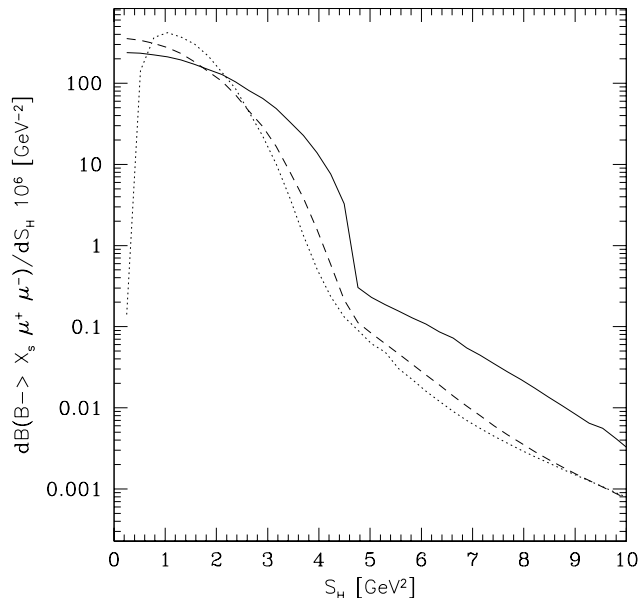


Figure 3: *Hadronic invariant mass spectrum in  $B \rightarrow X_s \ell^+ \ell^-$  including the perturbative and resonant ( $J/\psi, \psi', \dots$ ) contributions in the Fermi motion model. The solid, dotted and dashed curves correspond to the parameters  $(\lambda_1, \bar{\Lambda}) = (-0.3, 0.5), (-0.1, 0.4), (-0.15, 0.35)$  in  $(\text{GeV}^2, \text{GeV})$ , respectively.*

shape and normalization of the  $J/\psi$ -data, using the non-relativistic QCD (NRQCD) formalism for the inclusive color singlet and color octet charmonium production in  $B \rightarrow X_s J/\psi$  and the FM model [6]. The preferred FM parameters from this analysis are:  $(p_F, m_q) = (0.57 \text{ GeV}, 0.15 \text{ GeV})$ , where  $m_q$  only plays a role in determining the position of the peak but otherwise does not influence the small momentum tail of the  $J/\psi$  momentum distribution. This yields values of the parameter  $p_F$  which are consistent with the ones obtained in ref. [29]  $p_F = 0.54_{-0.15}^{+0.16}$ , GeV based on an analysis of the CLEO data on  $B \rightarrow X \ell \nu_\ell$  [28]. The central values of  $p_F$  in [29] as well as in [18] correspond to  $m_b^{\text{eff}} \simeq 4.6 \text{ GeV}$ , which is on the lower side of the present theoretical estimate of the  $m_b$  pole mass, namely  $m_b = 4.8 \pm 0.2 \text{ GeV}$  [20].

We have redone an analysis of the  $J/\psi$ -momentum distribution in the FM model which is shown in Fig. 1. As also discussed in [18], the low-momentum  $J/\psi$ , in particular in the region  $|k_{J/\psi}| \leq 0.6 \text{ GeV}$ , are problematic for inclusive decay models, including also the FM model (see Fig. 1). The measured  $|k_{J/\psi}|$ -spectrum appears to have a secondary bump; an inclusive spectrum behaving as a Gaussian tail or having a power-like behavior  $\propto |k_{J/\psi}|^{-\delta}$  in this region is hard put to explain this data. There are also suggestions in literature [30] that the spectrum in this region is dominated by the three-body decay  $B \rightarrow J/\psi \Lambda \bar{p}$  and hence the bump reflects the underlying dynamics of this exclusive decay. In view of this, we have taken out the first six points in the low- $|k_{J/\psi}|$  spectrum and fitted the FM model parameters in the rest of the  $|k_{J/\psi}|$ -spectrum. The three curves shown correspond to the

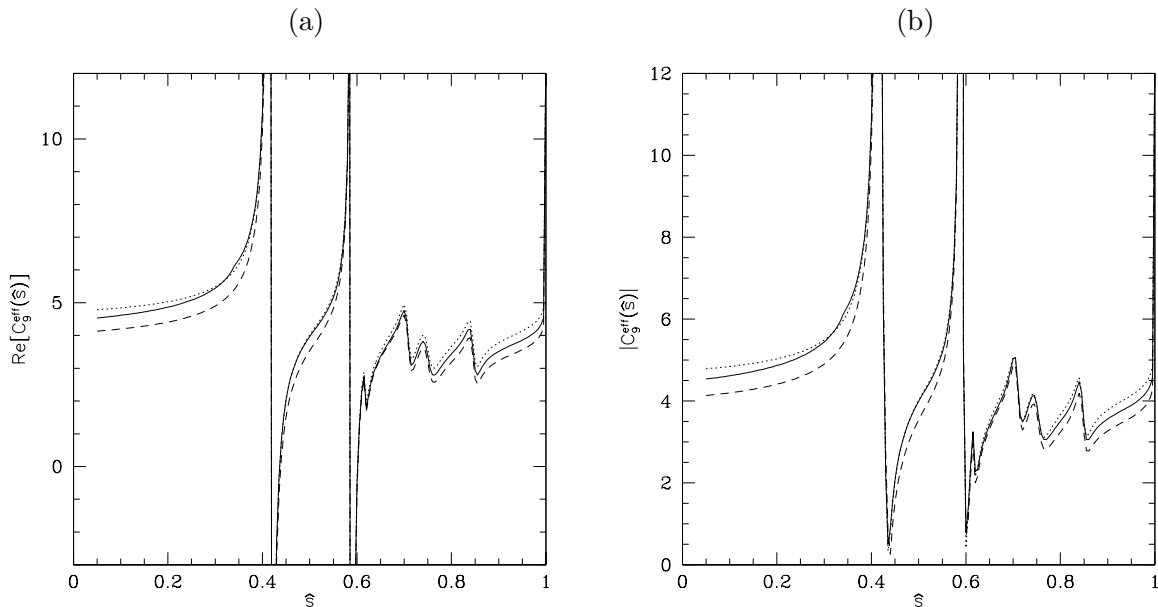


Figure 4: The real part (a) and the absolute value (b) of  $C_9^{\text{eff}}(\hat{s})$  are shown as a function of  $\hat{s}$ , where  $C_9^{\text{eff}}(\hat{s}) = C_9\eta(\hat{s}) + Y(\hat{s}) + Y_{\text{res}}(\hat{s})$ . The solid curve corresponds to  $Y(\hat{s})$  calculated using the perturbative  $c\bar{c}$  contribution  $g(\hat{m}_c, \hat{s})$  given in eq. (15), and the dotted curve corresponds to using  $\tilde{g}(\hat{m}_c, \hat{s})$  in eq. (28), with  $R_{\text{res}}(\hat{s})$  calculated in both cases using eq. (24). The dashed curve corresponds to using the Krüger-Sehgal approach [14] discussed in the text.

FM model parameters  $(p_F, m_q) = (0.45 \text{ GeV}, 0 \text{ GeV})$  (solid curve),  $(p_F, m_q) = (0.45 \text{ GeV}, 0.15 \text{ GeV})$  (dotted curve) and  $(p_F, m_q) = (0.50 \text{ GeV}, 0.15 \text{ GeV})$  (dashed curve). They all have reasonable  $\chi^2$ , with  $\chi^2/\text{dof} = 1.6, 1.6$  and  $1.1$ , respectively. Excluding also the seventh lowest point, the  $\chi^2$  improves marginally, with the resulting  $\chi^2$  being  $\chi^2/\text{dof} = 1.4, 1.4$  and  $0.94$ . Including the sixth point, the fits become slightly worse. However, they are all acceptable fits. It is interesting that the best-fit solution of the photon energy spectrum in  $B \rightarrow X_s + \gamma$ ,  $(p_F, m_q) = (0.45 \text{ GeV}, 0 \text{ GeV})$  [19], is also an acceptable fit of the  $|k_{J/\psi}|$ -data. The corresponding  $\lambda_1$ ,  $\bar{\Lambda}$  and  $m_b$  values from these two analyses are compatible within  $\pm 1\sigma$  with the HQET-based constraints from the semileptonic  $B$  decays [5], quoted above. Thus, the values in eq. (26) appear to be a reasonable guess of the FM model parameters. But, more importantly for the present study, the phenomenological profile of the LD contribution  $B \rightarrow X_s(J/\psi, \psi', \dots) \rightarrow X_s \ell^+ \ell^-$  presented here is certainly consistent with present data and theoretical constraints.

### 3.4 Effects of the Lorentz boost on the hadron spectra in $B \rightarrow X_s \ell^+ \ell^-$

We now discuss the  $B$ -meson wave function effects in the FM model on the hadron spectra in  $B \rightarrow X_s \ell^+ \ell^-$ . Since the resonances in  $B \rightarrow X_s \ell^+ \ell^-$  are in the dilepton invariant mass variable  $s$  and not in  $S_H$ , and noting that neither  $E_0$  (partonic energy) nor  $E_H$  are Lorentz-invariant parameters, it

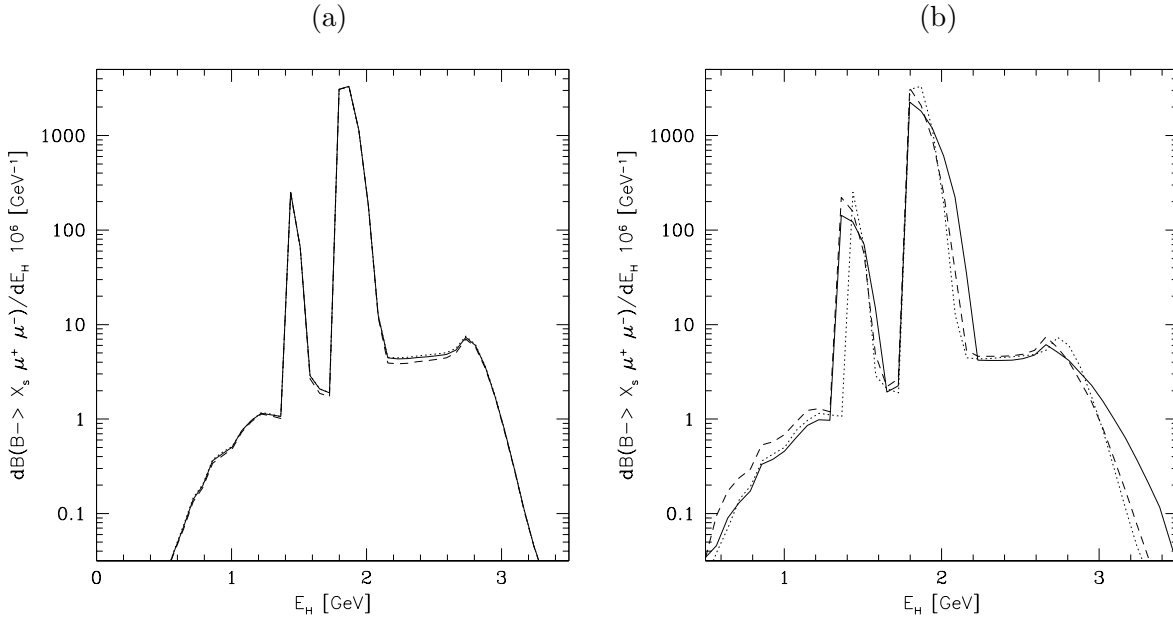


Figure 5: *Hadron energy spectrum in  $B \rightarrow X_s \ell^+ \ell^-$  including the resonant and perturbative contributions in the Fermi motion model. In (a), the FM model parameters are fixed at  $(\lambda_1, \bar{\Lambda}) = (-0.1 \text{ GeV}^2, 0.4 \text{ GeV})$ . The almost overlapping curves differ in the parametrization of  $C_9^{\text{eff}}(\hat{s})$  as depicted in Fig. (4). The solid curve is obtained using eq. (15) for  $g(\hat{m}_c, \hat{s})$ , the dotted curve is based on  $\tilde{g}(\hat{m}_c, \hat{s})$  given in eq. (28), with  $R_{\text{res}}(\hat{s})$  calculated in both cases using eq. (24), and the dashed curve corresponds to the Krüger-Sehgal approach [14]. In (b), the solid, dotted and dashed curves correspond to the parameters  $(\lambda_1, \bar{\Lambda}) = (-0.3, 0.5), (-0.1, 0.4), (-0.15, 0.35)$  in  $(\text{GeV}^2, \text{GeV})$ , respectively.*

is expected on general grounds that the effect of the Lorentz boost in the FM model on  $E_H$ - and  $S_H$ -distributions will be more marked than what was found on the invariant dilepton mass spectrum in [10]. We recall that for the dilepton invariant mass, the Lorentz boost involved in the FM model (Doppler shift) leaves the spectrum invariant and there is only a residual effect due to the fact that the  $b$ -quark mass in the parton model  $m_b$  and the effective  $b$ -quark mass in the FM model (called  $W(p)$  in [10] and  $m_b^{\text{eff}}$  here), are different quantities. This difference  $(W(p) - m_b)$  (mass defect) smears the dilepton invariant mass distribution, but being a subleading effect in  $1/m_b$  this effect is small. Not so in the hadron spectra. In the hadron energy spectrum, the  $c\bar{c}$ -resonances, which are narrowly peaked in the parton model, are broadened by the Lorentz boost of the FM model. To show this, the hadron energy spectrum in the FM model (dotted curve) is compared with the spectrum in the parton model (long-short dashed curve) in Fig. 2 for identical values of  $m_b$  and  $m_b^{\text{eff}}$ , taken as 4.85 GeV. In terms of the hadronic invariant mass, one finds that the resonant structure is greatly smeared. The reason for this behavior is that each  $q^2$ -bin contributes to a range of  $E_H$  and  $S_H$ . The different  $q^2$ -regions overlap in  $S_H$  resulting in a smearing of the resonances over a wide range. This can be seen in Fig. 3 for the hadronic invariant mass. Various curves illustrate the sensitivity of this spectrum on the FM

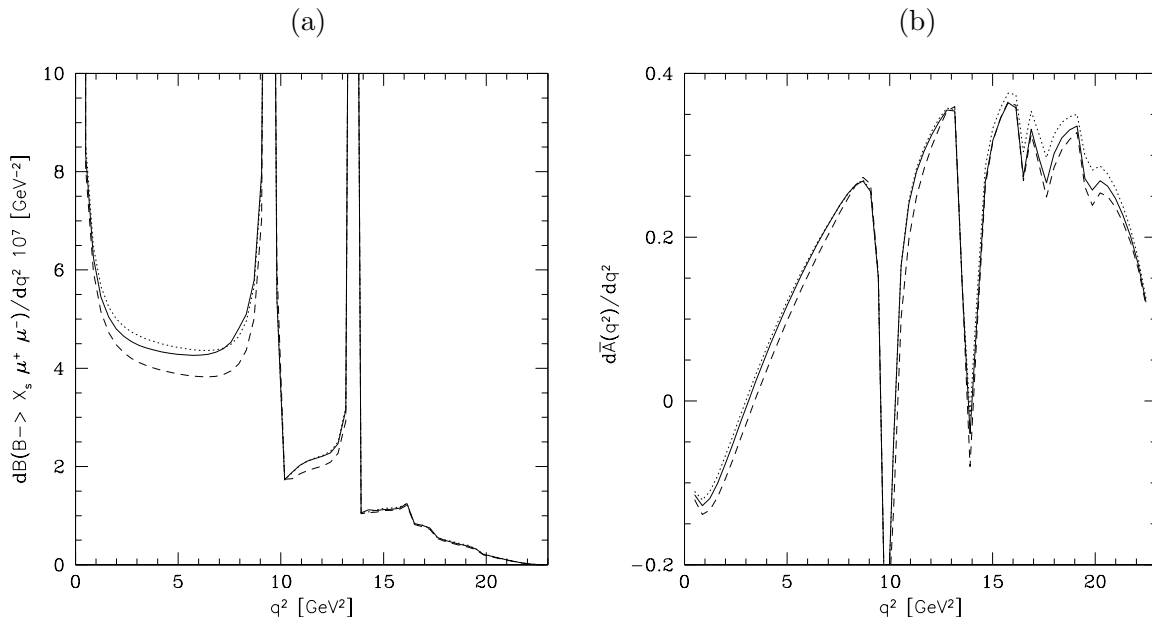


Figure 6: *Dilepton invariant spectrum (a) and the (normalized) Forward-Backward asymmetry (b) in  $B \rightarrow X_s \ell^+ \ell^-$  including the resonant and perturbative contributions in the Fermi motion model. The FM model parameters are fixed at  $(\lambda_1, \bar{\Lambda}) = (-0.1 \text{ GeV}^2, 0.4 \text{ GeV})$ . The solid curve is obtained using eq. (15) for  $g(\hat{m}_c, \hat{s})$ , the dotted curve is based on  $\tilde{g}(\hat{m}_c, \hat{s})$  given in eq. (28), with  $R_{res}(\hat{s})$  calculated in both cases using eq. (24), and the dashed curve corresponds to the Krüger-Sehgal approach [14].*

model parameters.

### 3.5 Ambiguities in adding LD and SD contributions in $B \rightarrow X_s \ell^+ \ell^-$

Since we are simply adding the short-distance (SD) and resonant charmonium amplitudes, it can not be ruled out that possibly some double counting has crept in in the coefficient  $C_9^{\text{eff}}(\hat{s})$  (once as a continuum  $c\bar{c}$  contribution and then again as  $J/\psi, \psi', \dots$  resonances). The question is whether the addition of the  $c\bar{c}$ -continuum and resonating pieces as being done here and in [10] compromises the resulting theoretical precision significantly. This can only be studied by comparing the theoretical scenario in question with other trial constructions advocated in the literature. For example, one could retain in the perturbative function  $g(\hat{m}_c, \hat{s})$  just the constant part in  $\hat{s}$  by replacing  $g(\hat{m}_c, \hat{s})$  by  $\tilde{g}(\hat{m}_c, \hat{s})$ , where

$$\tilde{g}(\hat{m}_c, \hat{s}) = -\frac{8}{9} \ln\left(\frac{m_b}{\mu}\right) - \frac{8}{9} \ln \hat{m}_c + \frac{8}{27}. \quad (28)$$

This function (with  $\mu = m_b$ ) has been proposed in [14,15] as an alternative representation of the  $c\bar{c}$  perturbative contribution and represents the (minimal) short-distance contribution. To study the difference numerically, we plot both the real part  $\text{Re } C_9^{\text{eff}}(\hat{s})$  and the absolute value  $|C_9^{\text{eff}}(\hat{s})|$  as functions of  $\hat{s}$  in Fig. 4 by using the complete perturbative expression for  $g(\hat{m}_c, \hat{s})$  in eq. (12) and  $\tilde{g}(\hat{m}_c, \hat{s})$

given in eq. (28). In both cases, the resonant contributions are included using eq. (24). As a third parametrization of  $C_9^{\text{eff}}(\hat{s})$ , we use the the approach of Krüger and Sehgal [14], based on dispersion relation <sup>1</sup> :

$$\begin{aligned}\text{Im } g(\hat{m}_c, \hat{s}) &= \frac{\pi}{3} R_{\text{had}}^{c\bar{c}}(\hat{s}) , \\ \text{Re } g(\hat{m}_c, \hat{s}) &= -\frac{8}{9} \ln \hat{m}_c - \frac{4}{9} + \frac{\hat{s}}{3} \int_{4\hat{m}_\pi^2}^{\infty} \frac{R_{\text{had}}^{c\bar{c}}(\hat{s}')}{\hat{s}'(\hat{s}' - \hat{s})} d\hat{s}' .\end{aligned}\quad (29)$$

The cross-section ratio  $R_{\text{had}}^{c\bar{c}}(\hat{s})$  in this approach is expressed as

$$R_{\text{had}}^{c\bar{c}}(\hat{s}) = R_{\text{cont}}^{c\bar{c}}(\hat{s}) + R_{\text{res}}^{c\bar{c}}(\hat{s}) , \quad (30)$$

where  $R_{\text{cont}}^{c\bar{c}}(\hat{s})$  and  $R_{\text{res}}^{c\bar{c}}(\hat{s})$  denote the contribution from the continuum and the narrow resonances, respectively. For the narrow resonances, the Breit-Wigner form given below in eq. (31) is used, whereas for the continuum part a parametrization of the  $e^+e^-$  annihilation data, taken from [31], is used.

$$R_{\text{res}}^{c\bar{c}}(\hat{s}) = \kappa \sum_{V_i=\psi(1s),\dots,\psi(6s)} \frac{9\hat{s} m_b^2 Br(V_i \rightarrow \ell^+\ell^-) \Gamma_{\text{total}}^{V_i} \Gamma_{\text{had}}^{V_i}}{\alpha^2 (\hat{s} m_b^2 - m_{V_i}^2)^2 + m_{V_i}^2 \Gamma_{\text{total}}^{V_i^2}} . \quad (31)$$

Note that the authors of [14] use  $\kappa = 2.35$  in their numerical analyses, which is slightly different than the one used in [10]. More importantly, this parametrization of  $R_{\text{res}}(\hat{s})$  has a different  $\hat{s}$ -dependence than the one given by eq. (24) and it incorporates the off-shell dependence of the effective  $\gamma^* \rightarrow V$  vertex, discussed in [13].

A number of comments on the curves shown in Fig. 4 and the resulting hadron energy and hadronic invariant mass distributions is in order.

- The results for both  $\text{Re } C_9^{\text{eff}}(\hat{s})$  and the absolute value  $|C_9^{\text{eff}}(\hat{s})|$  plotted as functions of  $\hat{s}$  show that the functions corresponding to [14] are lower than the ones used in [10], which, in turn, are lower than the ones obtained with the prescription given in [15]. However, one sees from Figs. 4 (a) and 4 (b) that the differences between these functions are numerically small.
- The three parametrizations discussed above give almost identical hadron spectra. The differences between these approaches in the  $E_H$ -spectrum are already difficult to see, as shown in Fig. 5 (a) where we have plotted the  $E_H$ -spectra in the FM model for the three parametrizations; the effect on the hadronic invariant mass is even less noticeable and hence is not shown. Quantitatively, the maximum difference in the hadron energy and the hadronic invariant mass spectra is 12.1(4.5)% and 4.1(2.5)%, respectively. The difference between the approaches in [10] and [14] is larger, as given by the first numbers, than the one between [10] and [15], given by the numbers in parentheses. However, these maximum differences occur only over a rather limited part of the phase space.

---

<sup>1</sup>The lower limit of the integral in eq. (29) must be below  $\hat{m}_{J/\psi}^2$  to include the dominant lowest  $c\bar{c}$  resonance contributions. We use  $4\hat{m}_\pi^2$  in consultation with F. Krüger.

- Other uncertainties on the hadronic distribution are much larger, see, for example, Fig. 5 (b) showing the sensitivity of the hadron energy spectra on the  $B$ -meson wave-function parameters. In comparison, the  $c\bar{c}$ -resonance/continuum related ambiguity is numerically small.

The results presented in Figs. 3 and 5 are the principal phenomenological results derived by us in this paper for the inclusive hadronic invariant mass and hadron energy spectra in the decay  $B \rightarrow X_s \ell^+ \ell^-$ , respectively, and are of direct experimental interest. The  $S_H$ -distribution and moments depend on the FM model parameters  $p_F$  and  $m_q$ . In the HQET approach, they depend on the parameters  $\bar{\Lambda}$  and  $\lambda_1$ . Since these parameters are already constrained by present data, the decay  $B \rightarrow X_s \ell^+ \ell^-$  can be gainfully used to determine them more precisely. This was discussed in [1,2]. Here, we have estimated the influence of the LD-resonant contribution.

### 3.6 Numerical Estimates of the Hadronic Moments in FM model and HQET

The similarity of the first two hadronic moments  $\langle X_H^n \rangle$ , with  $X = E, S$  and  $n = 1, 2$ , involving the SD-contribution in the decay  $B \rightarrow X_s \ell^+ \ell^-$  in the HQET and FM model descriptions was shown quantitatively in [2]. We include these numerical results here for comparison with the corresponding moments calculated including the LD-contribution in the FM model using the spectra which we have presented above. The moments based on the SD-contribution are defined as:

$$\langle X_H^n \rangle = \left( \int X_H^n \frac{d\mathcal{B}}{dX_H} dX_H \right) / \mathcal{B} \quad \text{for } X = S, E . \quad (32)$$

The moments  $\langle X_H^n \rangle_{\bar{c}c}$  are defined by taking into account in addition to the SD-contribution also the contributions from the  $c\bar{c}$  resonances. The values of the moments in both the HQET approach and the FM for  $n = 1, 2$  are shown in Table 4, with the numbers in the parentheses corresponding to the former. They are based on using the central values of the parameters given in Table 1, except for the values of  $\lambda_1$  and  $\bar{\Lambda}$  which are explicitly stated. The correspondence between the FM model and HQET parameters is given in eqs. (20). As already stated in [2], both the HQET and the FM model lead to strikingly similar results for the SD-contribution based hadronic moments shown in this table. However, the moments  $\langle X_H^n \rangle_{\bar{c}c}$  with  $X = S, E$  are significantly lower than their SD-counterparts  $\langle X_H^n \rangle$  calculated for the same values of the FM model parameters. This shows that the  $c\bar{c}$  resonances are important also in moments. The hadronic invariant mass spectra in  $B \rightarrow X_s \ell^+ \ell^-$  for both the SD and inclusive (LD+SD) contributions are expected to be dominated by multi-body states, with  $\langle S_H \rangle \simeq (1.5 - 2.1) \text{ GeV}^2$  and  $\langle S_H \rangle_{\bar{c}c} \simeq (1.2 - 1.5) \text{ GeV}^2$ .



	$\langle S_H \rangle$	$\langle S_H \rangle_{\bar{c}c}$	$\langle S_H^2 \rangle$	$\langle S_H^2 \rangle_{\bar{c}c}$
$(\lambda_1, \bar{\Lambda})$ in (GeV <sup>2</sup> , GeV)	(GeV <sup>2</sup> )		(GeV <sup>4</sup> )	
(-0.3, 0.5)	2.03 (2.09)	1.51	6.43 (6.93)	3.10
(-0.1, 0.4)	1.75 (1.80)	1.36	4.04 (4.38)	2.17
(-0.14, 0.35)	1.54 (1.49)	1.19	3.65 (3.64)	1.92
	$\langle E_H \rangle$	$\langle E_H \rangle_{\bar{c}c}$	$\langle E_H^2 \rangle$	$\langle E_H^2 \rangle_{\bar{c}c}$
$(\lambda_1, \bar{\Lambda})$ in (GeV <sup>2</sup> , GeV)	(GeV)		(GeV <sup>2</sup> )	
(-0.3, 0.5)	2.23 (2.28)	1.87	5.27 (5.46)	3.52
(-0.1, 0.4)	2.21 (2.22)	1.85	5.19 (5.23)	3.43
(-0.14, 0.35)	2.15 (2.18)	1.84	4.94 (5.04)	3.39

Table 4: *Hadronic spectral moments for  $B \rightarrow X_s \mu^+ \mu^-$  in the Fermi motion model (HQET) for the indicated values of the parameters  $(\lambda_1, \bar{\Lambda})$ .*

## 4 Branching Ratios and Hadron Spectra in $B \rightarrow X_s \ell^+ \ell^-$ with Cuts on Invariant Masses

In experimental searches for the decay  $B \rightarrow X_s \ell^+ \ell^-$ , the short-distance contribution (electroweak penguins and boxes) is expected to be visible away from the resonances. So, cuts on the invariant dilepton mass are imposed to stay away from the dilepton mass range where the charmonium resonances  $J/\psi$  and  $\psi'$  are dominant. For example, the cuts imposed in the recent CLEO analysis [7] given below are typical:

$$\begin{aligned}
\text{cut A} & : q^2 \leq (m_{J/\psi} - 0.1 \text{ GeV})^2 = 8.98 \text{ GeV}^2, \\
\text{cut B} & : q^2 \leq (m_{J/\psi} - 0.3 \text{ GeV})^2 = 7.82 \text{ GeV}^2, \\
\text{cut C} & : q^2 \geq (m_{\psi'} + 0.1 \text{ GeV})^2 = 14.33 \text{ GeV}^2.
\end{aligned} \tag{33}$$

The cuts  $A$  and  $B$  have been chosen to take into account the QED radiative corrections as these effects are different in the  $e^+e^-$  and  $\mu^+\mu^-$  modes. In the following, we compare the hadron spectra with and without the resonances after imposing these experimental cuts. For the low- $q^2$  cut for muons (cut  $A$ ), the hadron energy spectra and the hadronic invariant mass spectra are shown in Fig. 7 (a), (b) and Fig. 8 (a), (b), respectively. The results for the low- $q^2$  cut for electrons (cut  $B$ ), are shown in Fig. 7 (c), (d) and Fig. 8 (c), (d), respectively. Finally, the hadronic spectra for the high- $q^2$  cut (cut  $C$ ) for  $e^+e^-$  and  $\mu^+\mu^-$  can be seen in Fig. 7 (e), (f) for the hadronic energy and in Fig. 8 (e), (f) for the hadronic invariant mass. We see that the above cuts in  $q^2$  greatly reduce the resonance contributions. Hence, the resulting distributions essentially test the non-resonant  $c\bar{c}$  and short-distance contributions. These figures will be used later to quantify the model dependence of the integrated branching ratios in  $B \rightarrow X_s \ell^+ \ell^-$ .

As mentioned in [7], the dominant  $B\bar{B}$  background to the decay  $B \rightarrow X_s \ell^+ \ell^-$  comes from two semileptonic decays of  $B$  or  $D$  mesons, which produce the lepton pair with two undetected neutrinos. To suppress this  $B\bar{B}$  background, it is required that the invariant mass of the final hadronic state is less than  $t = 1.8 \text{ GeV}$ , which approximately equals  $m_D$ . We define the survival probability of the  $B \rightarrow X_s \ell^+ \ell^-$  signal after the hadronic invariant mass cut:

$$S(t) \equiv \left( \int_{m_X^2}^{t^2} \frac{d\mathcal{B}}{dS_H} dS_H \right) / \mathcal{B} , \quad (34)$$

and present  $S(t = 1.8 \text{ GeV})$  as the fraction of the branching ratio for  $B \rightarrow X_s \ell^+ \ell^-$  surviving these cuts in Table 5. To estimate the model dependence of this probability, we vary the FM model parameters. Concentrating on the SD piece, we note that the effect of this cut alone is that between 83% to 92% of the signal for  $B \rightarrow X_s \mu^+ \mu^-$  and between 79% to 90% of the signal in  $B \rightarrow X_s e^+ e^-$  survives, depending on the FM model parameters. The corresponding numbers for the inclusive spectrum including the SD and LD contribution is 96% to 99.7% for both the dimuon and dielectron case. This shows that while this cut removes a good fraction of the  $B\bar{B}$  background, it allows a very large fraction of the  $B \rightarrow X_s \ell^+ \ell^-$  signal to survive. However, this cut does not discriminate between the SD and (SD+LD) contributions, for which the cuts A - C are effective. The numbers for the survival probability  $S(t = 1.8 \text{ GeV})$  reflect that the hadronic invariant mass distribution of the LD-contribution is more steep than the one from the SD contribution.

With the additional cut A (B) imposed on the dimuon (dielectron) invariant mass, between 57% to 65% (57% to 68%) of the  $B \rightarrow X_s \ell^+ \ell^-$  signal survives the additional cut on the hadronic invariant mass for the SD contribution. However, as expected, the cuts A and B result in drastic reduction of the inclusive branching ratio for the decay  $B \rightarrow X_s \ell^+ \ell^-$ , as they effectively remove the dominant  $c\bar{c}$ -resonant part. In this case only 0.8% to 0.9% (1.0% to 1.2%) of the inclusive signal survives for the cut A (B). The theoretical branching ratios for both the dielectron and dimuon cases, calculated using the central values in Table 1 and the indicated values of  $\lambda_1$  and  $\bar{\Lambda}$  are also given in Table 5. As estimated in [2], the uncertainty on the branching ratios resulting from the errors on the parameters in Table 1 is about  $\pm 23\%$  (for the dielectron mode) and  $\pm 16\%$  (for the dimuon case). The wave-function-related uncertainty in the branching ratios is smaller, as can be seen in Table 5. This gives a fair estimate of the theoretical uncertainties on the partially integrated branching ratios from the  $B$ -meson wave function and  $c\bar{c}$  resonances. With the help of the theoretical branching ratio and the survival probability  $S(t = 1.8 \text{ GeV})$ , calculated for three sets of the FM parameters, the cross section can be calculated for all six cases:

- (i) no cut on the dimuon invariant mass [(SD) and (SD + LD)],
- (ii) no cut on the dielectron invariant mass [(SD) and (SD + LD)],
- (iii) cut A on the dimuon invariant mass [(SD) and (SD + LD)],
- (iv) cut B on the dielectron invariant mass [(SD) and (SD + LD)],
- (v) cut C on the dimuon invariant mass [(SD)

and (SD + LD)], (vi) cut C on the dielectron invariant mass [(SD) and (SD + LD)]. This table shows that with  $10^7 B\bar{B}$  events,  $\mathcal{O}(70)$  dimuon and  $\mathcal{O}(100)$  dielectron signal events from  $B \rightarrow X_s \ell^+ \ell^-$  should survive the CLEO cuts A and B, respectively, with  $m(X_s) < 1.8$  GeV. With the cut C, one expects an order of magnitude less events, making this region interesting for the LHC experiments which will have much higher  $B\bar{B}$  statistics. Given enough data, one can compare the experimental distributions in  $B \rightarrow X_s \ell^+ \ell^-$  directly with the ones presented here. The phenomenological success of the FM model in describing the energy spectra in  $B$  decays and its close proximity to HQET make us confident that the hadron spectra in  $B \rightarrow X_s \ell^+ \ell^-$  presented here should be good descriptions of the data.

#### 4.1 Hadronic Spectral Moments with Cuts in the FM

We have calculated the first two moments of the hadronic invariant mass in the FM model by imposing a cut  $S_H < t^2$  with  $t = 1.8$  GeV and an optional cut on  $q^2$ .

$$\langle S_H^n \rangle = \left( \int_{m_X^2}^{t^2} S_H^n \frac{d^2 \mathcal{B}_{cutX}}{dS_H dq^2} dS_H dq^2 \right) / \left( \int_{m_X^2}^{t^2} \frac{d^2 \mathcal{B}_{cutX}}{dS_H dq^2} dS_H dq^2 \right) \quad \text{for } n = 1, 2. \quad (35)$$

Here the subscript *cutX* indicates whether we evaluated  $\langle S_H \rangle$  and  $\langle S_H^2 \rangle$  with the cuts on the invariant dilepton mass as defined in eq. (33), or without any cut on the dilepton mass. The results are collected in Table 6. The moments given in Table 6 can be compared directly with the data to extract the FM model parameters. The entries in this table give a fairly good idea of what the effects of the experimental cuts on the corresponding moments in HQET will be, as the FM and HQET yield very similar moments for equivalent values of the parameters. The functional dependence of the hadronic moments on the HQET parameters taking into account the experimental cuts still remains to be worked out.

In the last row of Table 6 the value in percentage refers to the maximum uncertainty in  $\langle S_H^n \rangle$ , with  $n = 1, 2$ , resulting from different approaches to include the resonant  $c\bar{c}$  effects. We have calculated  $\langle S_H \rangle$  and  $\langle S_H^2 \rangle$  with all the cuts mentioned above for the three approaches for fixed  $(\lambda_1, \bar{\Lambda}) = (-0.1, 0.4)$  in  $\text{GeV}^2, \text{GeV}$ . Thus, for example,  $\langle S_H \rangle = (1.77 \pm 0.90\%) \text{ GeV}^2$  for Cut A. This uncertainty is much below the one due to the variations in the parameters  $\lambda_1$  and  $\bar{\Lambda}$ . Hence, the measurement of the hadronic moments can be used to determine these parameters.

## 5 Summary and Concluding Remarks

We summarize our results:

- We have presented the hadron spectra and moments in  $B \rightarrow X_s \ell^+ \ell^-$  including the resonant- $c\bar{c}$  contribution in the Fermi motion model [6]. This complements the description of the final states in  $B \rightarrow X_s \ell^+ \ell^-$  presented in [10], where the dilepton invariant mass spectrum and FB

FM parameters ( $\lambda_1, \bar{\Lambda}$ ) in (GeV <sup>2</sup> , GeV)	$\mathcal{B} \cdot 10^{-6}$ $\mu^+\mu^-$	$\mathcal{B} \cdot 10^{-6}$ $e^+e^-$	No $s$ -cut $\mu^+\mu^-$	No $s$ -cut $e^+e^-$	cut A $\mu^+\mu^-$	cut B $e^+e^-$	cut C $\mu^+\mu^-$	cut C $e^+e^-$
(-0.3, 0.5) [ $SD$ ]	5.8	8.6	83%	79 %	57%	57%	6.4%	4.5%
(-0.1, 0.4) [ $SD$ ]	5.7	8.4	93%	91 %	63%	68%	8.3%	5.8%
(-0.14, 0.35) [ $SD$ ]	5.6	8.3	92%	90 %	65%	67%	7.9%	5.5%
(-0.3, 0.5) [ $SD + LD$ ]	562.5	563.9	96%	96 %	0.8%	1.0%	0.06%	0.06%
(-0.1, 0.4) [ $SD + LD$ ]	564.0	565.6	99.7%	99.7%	0.8%	1.1%	0.08%	0.08%
(-0.14, 0.35) [ $SD + LD$ ]	566.5	568.2	99%	99 %	0.9%	1.2%	0.08%	0.08%

Table 5: *Branching ratios and survival probabilities for  $B \rightarrow X_s \ell^+ \ell^-$ ,  $\ell = \mu, e$  for different FM model parameters evaluated from the  $SD$  and [ $SD + LD$ ] contributions. The branching ratios without experimental cuts are given in the second and third columns. The values given in percentage in the fourth to eleventh columns represent the survival probability  $S(t = 1.8 \text{ GeV})$  defined in eq. (34) without any cut on the dilepton invariant mass and for three different cuts as defined in eq. (33).*

asymmetry were worked out in both the HQET and FM model approaches. We find that the hadron energy spectrum is stable against variation of the FM model parameters. However, the hadronic invariant mass is sensitive to the input parameters. This dependence was already studied for the  $SD$ -contribution in [1,2] both in the context of the FM model and HQET.

- We have quantitatively studied the uncertainties related to the implementation of the resonant and non-resonant parts in the coefficient  $C_9^{\text{eff}}(\hat{s})$  in  $B \rightarrow X_s \ell^+ \ell^-$ . The numerical differences between the approach followed in [10] and the alternative ones, discussed in [14] and [15], are found to be small in the dilepton invariant mass spectrum and negligible in the hadron energy and invariant mass spectra and spectral moments. In contrast, theoretical spectra are found to be more sensitive to the parameters  $\lambda_1$  and  $\bar{\Lambda}$ .
- We have studied the hadron spectra by imposing the experimental cuts designed to suppress the resonant  $c\bar{c}$  contributions, as well as the dominant  $B\bar{B}$  background leading to the final state  $B\bar{B} \rightarrow X_s \ell^+ \ell^-$  (+ missing energy). In particular, the survival probability of the  $B \rightarrow X_s \ell^+ \ell^-$ -signal resulting from imposing a cut on the hadronic invariant mass  $S_H < 3.24 \text{ GeV}^2$ , as used in the CLEO analysis, is estimated and its parametric dependence studied. We have shown that the cuts such as the ones used in [7] effectively suppress the resonant contribution. Thus, the cut spectra essentially test the physics of the short-distance (and non-resonant  $c\bar{c}$ ) contribution, which can be systematically studied in perturbation theory and HQET.

We hope that this work which provides a detailed theoretical profile of the hadron spectra in the decay  $B \rightarrow X_s \ell^+ \ell^-$  will be helpful in experimental searches of the rare decay  $B \rightarrow X_s \ell^+ \ell^-$ . The distributions presented here will allow direct comparison of data with SM and will be useful in

FM parameters ( $\lambda_1, \bar{\Lambda}$ ) GeV <sup>2</sup> , GeV	No $s$ -cut $\mu^+\mu^-$		No $s$ -cut $e^+e^-$		cut A $\mu^+\mu^-$		cut B $e^+e^-$		cut C $\ell^+\ell^-$	
	$\langle S_H \rangle$	$\langle S_H^2 \rangle$	$\langle S_H \rangle$	$\langle S_H^2 \rangle$	$\langle S_H \rangle$	$\langle S_H^2 \rangle$	$\langle S_H \rangle$	$\langle S_H^2 \rangle$	$\langle S_H \rangle$	$\langle S_H^2 \rangle$
	GeV <sup>2</sup>	GeV <sup>4</sup>	GeV <sup>2</sup>	GeV <sup>4</sup>	GeV <sup>2</sup>	GeV <sup>4</sup>	GeV <sup>2</sup>	GeV <sup>4</sup>	GeV <sup>2</sup>	GeV <sup>4</sup>
(−0.3, 0.5)	1.47	2.87	1.52	3.05	1.62	3.37	1.66	3.48	0.74	0.69
(−0.1, 0.4)	1.57	2.98	1.69	3.37	1.80	3.71	1.88	3.99	0.74	0.63
(−0.14, 0.35)	1.31	2.34	1.38	2.55	1.47	2.83	1.52	2.97	0.66	0.54
(−0.3, 0.5) <sub>tot</sub>	1.41	2.61	1.41	2.62	1.61	3.32	1.66	3.47	0.74	0.68
(−0.1, 0.4) <sub>tot</sub>	1.35	2.14	1.36	2.15	1.77	3.60	1.87	3.94	0.74	0.62
(−0.14, 0.35) <sub>tot</sub>	1.17	1.84	1.18	1.85	1.45	2.76	1.51	2.95	0.66	0.54
$\Delta$	0.15%	0.19%	0.22%	0.42%	0.90%	1.56%	0.32%	0.58%	0.01%	0.32%

Table 6: Spectral moments  $\langle S_H \rangle$  and  $\langle S_H^2 \rangle$  for  $B \rightarrow X_s \ell^+ \ell^-$ ,  $\ell = \mu, e$  for different FM model parameters and a hadronic invariant mass cut  $S_H < 3.24 \text{ GeV}^2$  are given in the second to fifth columns. The values in the sixth to eleventh columns have additional cuts on the dilepton invariant mass spectrum as defined in eq. (33). The  $S_H$ -moments with cuts are defined in eq. (35). Entries in the first three rows are calculated using the SD-contribution alone. The subscript  $tot = SD + LD$  denotes that both the short and the long distance contribution are included in these moments. The values of  $\Delta$  given in the last row represent the maximum uncertainty on the spectral moments (in %) resulting from the three approaches to take into account the continuum/ $c\bar{c}$ -resonant contributions discussed in the text.

estimating the effects of various experimental cuts on the hadronic and dilepton invariant masses and hadron energy, which will be invoked in experimental analyses. Finally, this work underscores the importance of systematically improving the theoretical precision of the hadron spectra and spectral moments in the SD-contribution in the decay  $B \rightarrow X_s \ell^+ \ell^-$  beyond what has been already done in [1,2], as the theoretical uncertainties from the LD-contributions can be brought under control by judicious experimental cuts.

## Acknowledgements

We would like to thank Frank Krüger for helpful correspondence on the implementation of the charmonium contribution given in [14]. We also thank Christoph Greub for useful discussions.

## References

- [1] A. Ali and G. Hiller, preprint DESY 98-025, hep-ph/9803407, to appear in Phys. Rev. D.
- [2] A. Ali and G. Hiller, preprint DESY 98-030, hep-ph/9803428, to appear in Phys. Rev. D.

- [3] J. Chay, H. Georgi and B. Grinstein, Phys. Lett. **B247** (1990) 399; I.I. Bigi, N.G. Uraltsev and A.I. Vainshtein, Phys. Lett. **B293** (1992) 430 [E. **B297** (1993) 477]; I.I. Bigi et al., Phys. Rev. Lett. **71** (1993) 496; B. Blok et al., Phys. Rev. **D49** (1994) 3356 [E. **D50** (1994) 3572].
- [4] A. Manohar and M. B. Wise, Phys. Rev. **D49** (1994) 1310.
- [5] M. Gremm, A. Kapustin, Z. Ligeti and M.B. Wise, Phys. Rev. Lett. **77** (1996) 20.
- [6] A. Ali and E. Pietarinen, Nucl. Phys. **B154** (1979) 519;  
G. Altarelli et al., Nucl. Phys. **B208** (1982) 365.
- [7] S. Glenn et al. (CLEO Collaboration), Phys. Rev. Lett. **80** (1998) 2289.
- [8] M. Bauer and B. Stech, Phys. Lett. **B152** (1985) 380; M. Bauer, B. Stech and M. Wirbel, Z. Phys. **C34** (1987) 103.
- [9] T.E. Browder, K. Honscheid and D. Pedrini, Ann. Rev. Nucl. Part. Sci. **46** (1996) 395.
- [10] A. Ali, L. T. Handoko, G. Hiller and T. Morozumi, Phys. Rev. **D55** (1997) 4105.
- [11] A. Ali, T. Mannel and T. Morozumi, Phys. Lett. **B273** (1991) 505.
- [12] C.S. Lim, T. Morozumi and A.I. Sanda, Phys. Lett. **B218** (1989) 343; N.G. Deshpande, J. Trampetic and K. Panose, Phys. Lett. **B214** (1988) 467; Phys. Rev. **D39** (1989) 1461; P.J. O'Donnell and H.K.K. Tung, Phys. Rev. **D43** (1991) 2067.
- [13] M.R. Ahmady, Phys. Rev. **D53** (1996) 2843; C.-D. Lü and D.-X. Zhang, Phys. Lett. **B397** (1997) 279.
- [14] F. Krüger and L.M. Sehgal, Phys. Lett. **B380** (1996) 199.
- [15] Z. Ligeti, I.W. Stewart and M.B. Wise, Phys. Lett. **B420** (1998) 359.
- [16] D. Melikhov, N. Nikitin and S. Simula, Phys. Rev. **D57** (1998) 6814; preprint hep-ph/9803343.
- [17] R. Balest et al. (CLEO Collaboration), Phys. Rev. **D52** (1995) 2661, and references quoted therein for earlier measurements.
- [18] W.F. Palmer, E.A. Paschos and P.H. Soldan, Phys. Rev. **D56** (1997) 5794.
- [19] A. Ali and C. Greub, Phys. Lett. **B361** (1995) 146.
- [20] M. Neubert, C. Sachrajda, Nucl. Phys. **B483** (1997) 339.

- [21] A. Czarnecki, M. Jezabek and J. H. Kühn, Acta. Phys. Pol. **B20** (1989) 961;  
M. Jezabek and J. H. Kühn, Nucl. Phys. **B320** (1989) 20.
- [22] A. J. Buras and M. Münz, Phys. Rev. **D52** (1995) 186.
- [23] M. Misiak, Nucl. Phys. **B393** (1993) 23 [E. **B439** (1995) 461].
- [24] Z. Ligeti and M.B. Wise, Phys. Rev. **D53** (1996) 4937.
- [25] M. Neubert and B. Stech, preprint CERN-TH-97-099, hep-ph/9705292.
- [26] A. Ali and C. Greub, Z. Phys. **C49** (1991) 431; Phys. Lett. **B259** (1991) 182.
- [27] M.S. Alam et al. (CLEO Collaboration), Phys. Rev. Lett. **74** (1995) 2885.
- [28] J. Bartelt et al. (CLEO Collaboration), CLEO/CONF 93-19;  
B. Barish et al. (CLEO Collaboration), Phys. Rev. Lett. **76** (1996) 1570;  
R.Wang, Ph. D. Thesis, University of Minnesota (1994).
- [29] D.S. Hwang, C.S. Kim and W. Namgung, Z. Phys. **C60** (1996) 107; Phys. Rev. **D54** (1996) 5620.
- [30] S.J. Brodsky and F.S. Navarra, Phys. Lett. **B411** (1997) 152.
- [31] H. Burkhardt and B. Pietrzyk, Phys. Lett. **B356** (1995) 398.

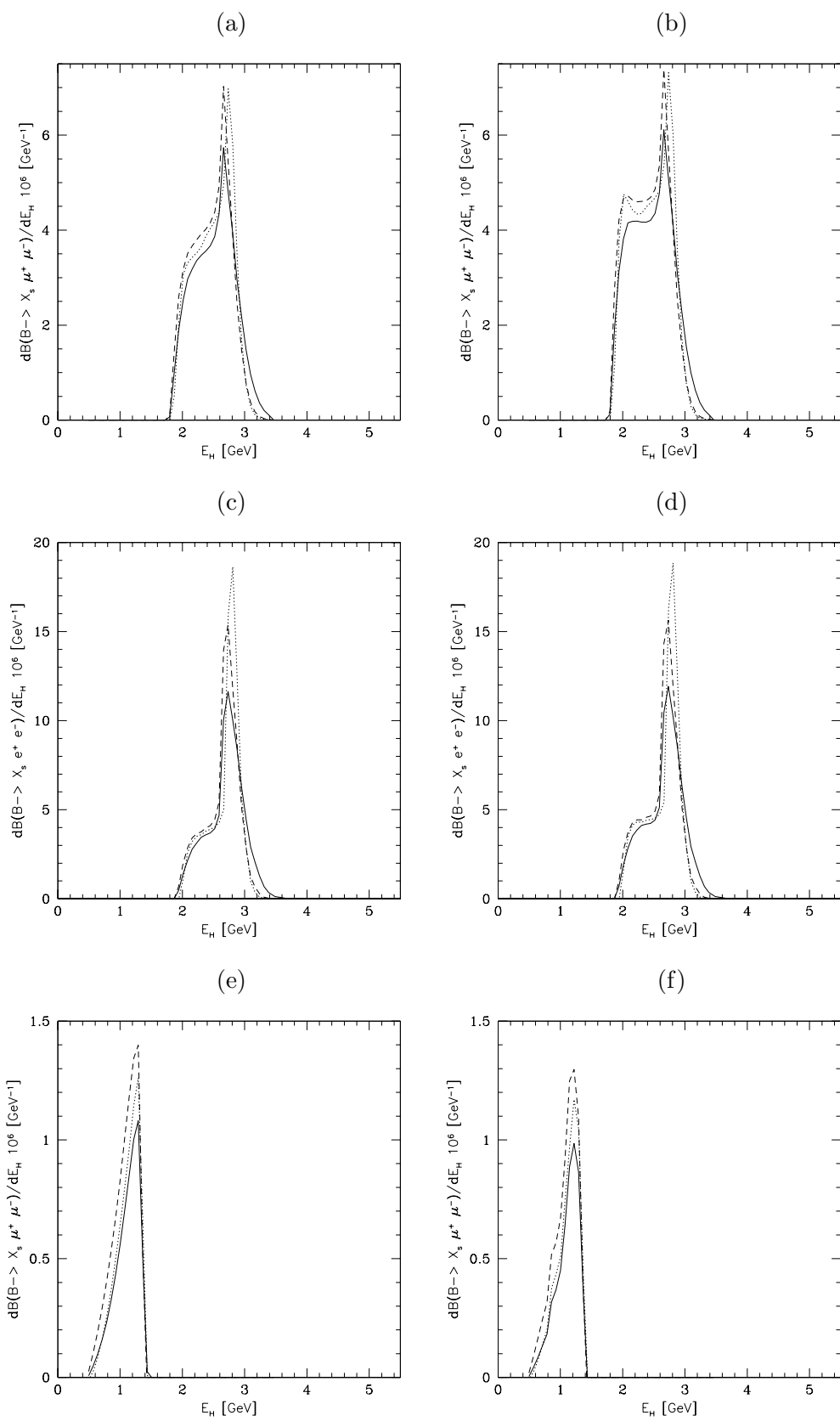


Figure 7: Hadron energy spectrum in  $B \rightarrow X_s \ell^+ \ell^-$  in the Fermi motion model with the cuts on the dilepton mass defined in eq. (33); (a),(c),(e) without and (b),(d),(f) with the  $c\bar{c}$ -resonance contribution corresponding to cut A,B,C, respectively. The solid, dotted and dashed curves correspond to the parameters  $(\lambda_1, \bar{\Lambda}) = (-0.3, 0.5), (-0.1, 0.4), (-0.15, 0.35)$  in  $(\text{GeV}^2, \text{GeV})$ , respectively.



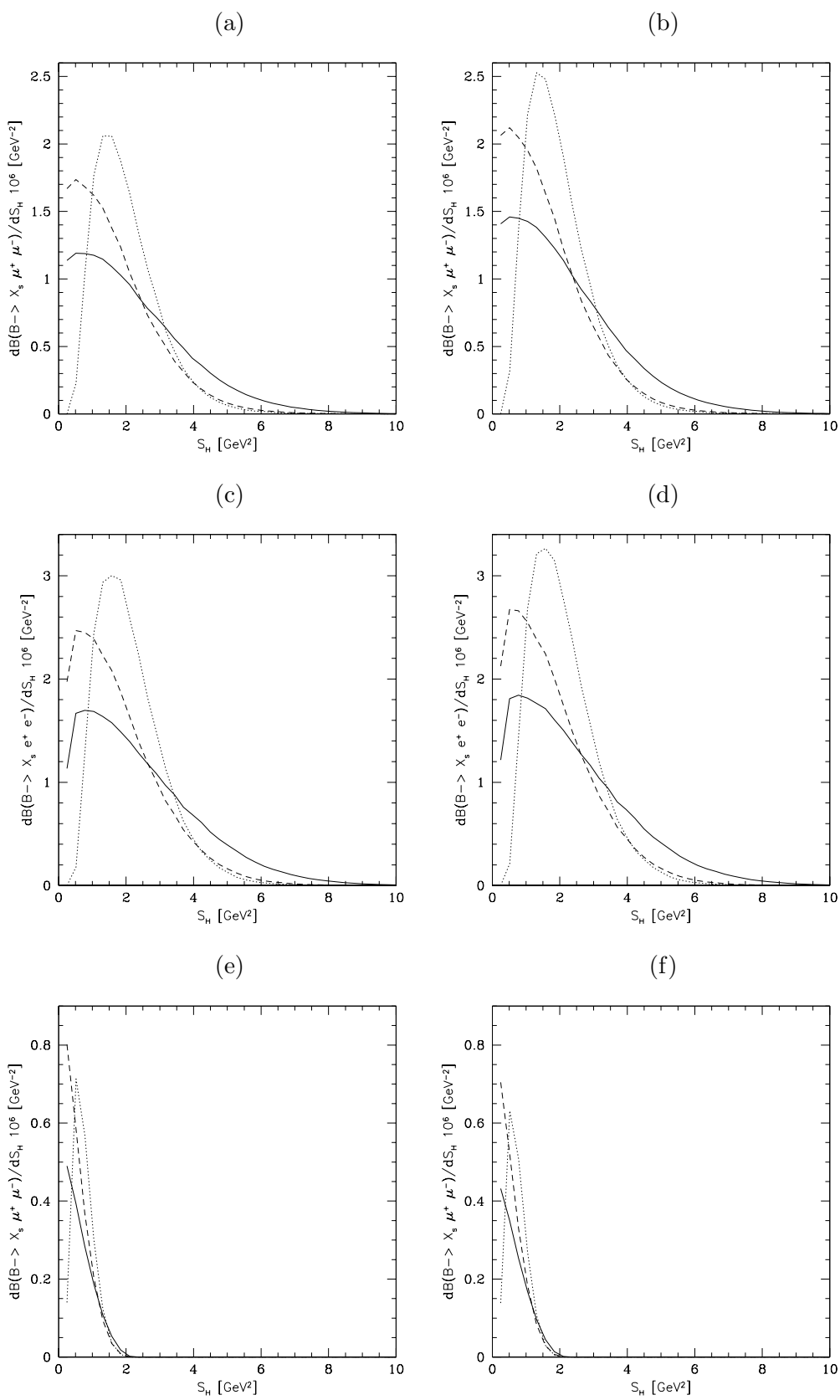


Figure 8: *Hadronic invariant mass spectrum in  $B \rightarrow X_s \ell^+ \ell^-$  in the Fermi motion model with the cuts on the dilepton mass defined in eq. (33); (a),(c),(e) without and (b),(d),(f) with the  $c\bar{c}$ -resonance contribution corresponding to cut A,B,C, respectively. The solid, dotted and dashed curves correspond to the parameters  $(\lambda_1, \bar{\Lambda}) = (-0.3, 0.5), (-0.1, 0.4), (-0.15, 0.35)$  in  $(\text{GeV}^2, \text{GeV})$ , respectively.*